Journal of Membrane Science 531 (2017) 138–147

Contents lists available at ScienceDirect

Journal of Membrane Science

journal homepage: www.elsevier.com/locate/memsci

# Predicting performance of constant flow depth filtration using constant pressure filtration data

Stephen Goldrick[a,1], Adrian Joseph[a,1], Michael Mollet[b], Richard Turner[c], David Gruber[c], Suzanne S. Farid[a], Nigel J. Titchener-Hooker[a,*]

[a] The Advanced Centre of Biochemical Engineering, Department of Biochemical Engineering, University College London, Gordon Street, WC1H 0AH London, United Kingdom
[b] MedImmune, One MedImmune Way, Gaithersburg, MD 20878, United States
[c] MedImmune, Milstein Building, Granta Park, Cambridge CB21 6GH, United Kingdom

ARTICLE INFO

*Keywords:*
Constant flow
Constant pressure
Depth filtration
Filter sizing
Mammalian cell
Fouling models

ABSTRACT

This paper describes a method of predicting constant flow filtration capacities using constant pressure datasets collected during the purification of several monoclonal antibodies through depth filtration. The method required characterisation of the fouling mechanism occurring in constant pressure filtration processes by evaluating the best fit of each of the classic and combined theoretical fouling models. The optimised coefficients of the various models were correlated with the corresponding capacities achieved during constant flow operation at the specific pressures performed during constant pressure operation for each centrate. Of the classic and combined fouling models investigated, the Cake-Adsorption fouling model was found to best describe the fouling mechanisms observed for each centrate at the various different pressures investigated. A linear regression model was generated with these coefficients and was shown to predict accurately the capacities at constant flow operation at each pressure. This model was subsequently validated using an additional centrate and accurately predicted the constant flow capacities at three different pressures (0.69, 1.03 and 1.38 bar). The model used the optimised Cake-Adsorption model coefficients that best described the flux decline during constant pressure operation. The proposed method of predicting depth filtration performance proved to be faster than the traditional approach whilst requiring significantly less material, making it particularly attractive for early process development activities.

## 1. Introduction

The market for therapeutic monoclonal antibodies (mAb) has seen unprecedented growth in recent years and this expansion is predicted to continue over the next decade [1]. To meet product supply for this increasing market and to ensure potential new drug candidates are manufactured effectively, pharmaceutical and biotechnology companies are required to operate across a wide range of scales, including large-scale manufacturing performed in vessels up to 20,000 L in addition to research development activities carried out using small or micro-scale systems. One of the challenges of operating at multiple scales is the need for flexible and scalable downstream processing unit operations. Depth filtration is an adaptable and scalable unit operation that has gained wide acceptance as the technique of choice for the clarification of mammalian cell culture broth post-centrifugation [2]. Accurate estimations of the optimum filter sizing of this key unit operation are critical. Over-sizing of the filter is uneconomic and under-sizing of the filter can result in process-related issues such as increased fouling in subsequent chromatographic stages thus shortening column lifetime and efficiency [3,4] or filter blockage resulting in loss of material. For constant flow operation the optimum filter area or capacity is defined as the cumulative volume of material filtered until a maximum pressure is reached [5] whereas the capacity for constant pressure is determined as the volume of material processed before a minimum flow rate is reached [6]. The optimum capacity of this unit operation is difficult to predict and can be influenced by a large number of parameters, including mode of operation, type of cell line, level of aggregates, cell culture conditions and centrifuge operating conditions [2]. Typically in an industrial environment, depth filtration trials are performed in constant flow mode on a scale-down mimic that predicts

* Correspondence to: The Advanced Centre of Biochemical Engineering, Department of Biochemical Engineering, University College London, Bernard Katz Building, London WC1E 6BT, United Kingdom.
*E-mail address:* nigelth@ucl.ac.uk (N.J. Titchener-Hooker).
[1] Both authors contributed equally to this work.

http://dx.doi.org/10.1016/j.memsci.2017.03.002
Received 25 August 2016; Received in revised form 24 February 2017; Accepted 1 March 2017
Available online 03 March 2017

**Nomenclature**

| | |
|---|---|
| $a$ | cake model coefficient (L $m^{-2}$) |
| $b$ | cake model exponential coefficient (m) |
| $A$ | available membrane frontal area ($m^2$) |
| $CF_{Cap,i}$ | filter capacity at constant flow for a given pressure (L $m^{-2}$) |
| $J$ | flux (L $m^2$ $h^{-1}$) |
| $J_v(0)$ | initial flux (L $m^2$ $h^{-1}$) |
| $J_v(t)$ | flux relative to available membrane area (L $m^2$ $h^{-1}$) |
| $K_A$ | complete blocking constant ($m^2$ $L^{-1}$) |
| $K_C$ | cake filtration constant ($m^2$ $L^{-1}$) |
| $K_{Com}$ | complete blocking constant ($m^2$ $L^{-1}$) |
| $K_I$ | intermediate blocking constant ($m^2$ $L^{-1}$) |
| $K_S$ | standard blocking constant ($m^2$ $L^{-1}$) |
| *LMH* | liters per meter per hour (L $m^{-2}$ $h^{-1}$) |
| $P$ | pressure (bar) |
| $R_{filter}$ | specific resistance to filtration ($m^{-1}$) |
| $R^2$ | coefficient of determination |
| $t$ | time (h) |
| $V$ | volume filtered ($m^3$) |

*Greek letters*

| | |
|---|---|
| $\alpha_O$ | Cake-Adsorption model coefficient (L $m^{-2}$ $h^{-1}$) |
| $\alpha_{1,2,}$ | Cake-Adsorption model coefficients ($L^2$ $m^{-4}$ $h^{-1}$) |
| $\alpha_{3,4}$ | Cake-Adsorption model coefficients ($L^4$ $m^{-6}$ h) |
| $\mu$ | solution viscosity (Pa s) |

the capacity at large-scale for each material tested. One of the problems of this approach is that it is time-consuming and material-intensive, particularly in comparison to capacity predictions performed in constant pressure mode. Fundamentally constant pressure and constant flow are operated differently. In constant flow operation a positive displacement pump is required to ensure the constant flow is maintained throughput the run. The pressure drop across the filter increases to maintain this constant flow due to foulant build up with time. In contrast, during constant pressure operation the initial flux through the filter is relatively high and decreases gradually as the filter fouls resulting in the hydrodynamic conditions at the filter surface changing over time [7]. This initial high flux can result in severe fouling [8] and therefore subsequently reduce the overall capacity of the filter. Hence the majority of biopharmaceutical processes operate in constant flow mode to maximize the available filter area. Miller et al. [7] demonstrated comparable fouling behavior between constant flow and constant pressure operation during dead-end ultrafiltration of an emulsified oil for low constant flow operation ( < 62 LMH) with deviations between the modes of operation found for flows about this value. Furthermore, Bolton et al. [9] and Chellam and Xu [10] demonstrated comparable fouling characteristics between the two modes of operation during the dead-end ultrafiltration of various materials ranging from antibody preparations to bacteria. Little research has investigated the conversion of constant pressure to constant flow operation for depth filtration.

Understanding membrane fouling remains a major challenge due to the multiple factors influencing this highly complex mechanism. Upstream processing conditions including cell viability and centrifuge operation can greatly influence the feed material onto a primary recovery depth filter resulting in significantly varied filtration properties [11]. Furthermore, the filters typically have an anisotropic pore structure resulting in various fouling mechanisms from deposition to adsorption of solutes to the membrane surface, cake layer formation, concentration polarisation and build-up of osmotic pressure [7]. In an attempt to simplify these highly complicated mechanisms various mathematical models have been applied to quantify the observed fouling. A limitation of these blocking models is that they are semi-empirical and assume the fouling mechanism is solely related to the physical blockage of the pores or inner pore walls as a result of the particles depositing onto the surface [12]. However, his generalisation has been widely implemented and successfully approximated the observed fouling during dead-end microfiltration [8,13–15], ultrafiltration [16,17] and depth-filtration [18,19]. The four classic models outlined in the literature are referenced as Complete blocking, Standard blocking, Cake filtration and Intermediate blocking [15]. Combination models have also been investigated which incorporate two or more of the classic models in conjunction. These have been shown to describe better the observed fouling in filters where classic models fail [17]. Most research has focused on the application of these mathematical models to define the fouling properties of proteins in dead-end microfiltration systems during constant pressure operation [9,13,15] or ultra-filtration [17,18]. Depth filtration operates slightly differently than these absolute filters and mainly retains the particles in the filter media, however these fouling models have been successfully demonstrated to model the observed fouling [19]. Sampath et al. [15] showed that these mathematical models can characterise the fouling of depth filters during the loading of a *Pichia pastoris* fermentation during constant pressure operation. Hlavacek and Bouchet [16] implemented the models to explore the fouling behaviours at constant flow and demonstrated the ability of the intermediate model to fit the pressure increase of bovine serum albumin (BSA) solutions filtered through various different membrane types. Similarly, Ho and Zydney [13] modelled constant flow microfiltration of protein, while Chellam and Xu [10] used these blocking laws to analyse the constant flow microfiltration of colloids. As depth filtration post centrifugation is the primary clarification method for large-scale mammalian cell manufacturing there is a need to investigate the various fouling modes that occur during both constant flow and constant pressure operation.

The ability to translate across constant flow and constant pressure models in filtration studies would be a major step forward and result in significant savings of time and valuable test materials for filter sizing studies. Bolton et al. [9] investigated the transition between these two modes of operation on dead-end microfiltration through characterisation of a bovine serum albumin foulant on a membrane filter. They found that the parameter coefficients of various theoretical models used to fit the flux decline during constant pressure operation could be used within the constant flow model to predict the observed pressure increase. However, with this method some models require calculation of the initial pressure drop for constant flow operation or the initial flux decline for constant pressure operation to generate predictions in the different mode.

Our study provides a methodology to accurately predict the capacity of depth filtration operated under constant flow utilising only constant pressure flux decline data. The flux decline of a wide range of industrially relevant centrates was characterised under constant pressure operation by evaluating the fit of various theoretical fouling models. Subsequently, constant flow experiments were conducted to determine the capacity of each of the centrates investigated. The model was found to be highly robust based on a low root mean square error for cross-validation. Additional experiments were performed to validate further the model and demonstrate its ability to predict accurately capacity at constant flow using data performed at constant pressure while also using significantly less material. This method may be highly beneficial at an early stage in the development of new molecules or proteins where material and time resources for process studies are often in short supply.

## 2. Theoretical considerations

In depth filtration the rate of filter fouling can be described by the generalised form of Darcy's Law:

$$J_v = \frac{1}{A}\frac{dV}{dt} \approx \frac{\Delta P}{R_{filter}\mu} \quad (1)$$

where $J_v$ is the permeate flux defined by the flow rate per unit area of $A$ with $V$ and $t$ representing the volume and time respectively. The pressure drop across the filter, $\Delta P$, depends on the viscosity of the material, $\mu$, and the specific filter resistance, $R_{filter}$. During constant flow operation ($\Delta J_v$=0), the increase in pressure during fouling is represented as:

$$\Delta P = J_v R_{filter}\mu \quad (2)$$

Whereas during constant pressure operation ($\Delta P$ is fixed) the decrease in flux is represented by:

$$\Delta J_v = \frac{\Delta P}{R_{filter}\mu} \quad (3)$$

Both the viscosity and equivalent filter resistance are specific to the material being filtered and dependent on the filter type and pore size. In both modes of operation the increase in filter resistance ($R_{filter}$) during dead-end filtration relates to filter fouling as a result of particle retention on the surface and inner walls of the filter, cake layer formation, concentration polarisation in addition to other microscopic fouling mechanisms. The increase in filter resistance results in a reduction in flux during constant pressure operation whereas a pressure increase is observed during constant flow operation. To characterise the observed fouling, researchers have relied on four classical fouling models; Cake filtration, Complete, Intermediate and Standard blocking. These models are semi-empirical and are highly dependent on the ratio of the particle size of the cell culture material to filter pore size [20]. Filter resistance is increased by large particles retained on the surface that completely block (Complete blocking) or partially block the available pores (Intermediate blocking). This filter foulant can increase with time as more material is filtered and the particles can form a cake layer (Cake filtration) further increasing the filter resistance. Small particles in the material relative to the filter pore size can deposit within the pore structure (Standard blocking or Adsorption) reducing the radius of the pore and therefore restricting the volume throughput of the filter.

The primary blocking models were originally defined by Hermans and Bredee [21] in 1935 and have more recently gained significant interest based on their application to dead-end microfiltration of protein solutions by Bowen et al. [15] and Ho and Zydney [13]. These models are defined by Bowen et al. [9] as Complete blocking, Intermediate blocking, Standard blocking and Cake filtration.

Complete blocking occurs when each particle arriving at the filter participates in blocking the pores of the membrane and is defined by Eq. (4) where $K_{Com}$ is the fouling coefficient for the Complete blocking model and $J_v(0)$ is the initial permeate flux.

$$\text{Complete blocking model: } J_v(t) = J_v(0)e^{-K_{Com}J_v(0)t} \quad (4)$$

Cake filtration occurs when the particles form a resistant layer on top of the filter, this layer increases in depth as new particles arrive at the filter and is defined as Eq. (5) where $K_C$ is the fouling coefficient for the Cake filtration model.

$$\text{Cake filtration model: } J_v(t) = \frac{J_v(0)}{\sqrt{1+K_C J_v(0)t}} \quad (5)$$

Intermediate blocking assumes that some particles arriving at the filter will directly block a portion of the available area while other particles will only participate in partial blockage of the pores and is defined as Eq. (6) where $K_I$ is the fouling coefficient for the Intermediate blocking model.

$$\text{Intermediate blocking model: } J_v(t) = \frac{J_v(0)}{1+K_I J_v(0)t} \quad (6)$$

Standard blocking assumes that particles deposit onto the internal walls of the pores. As further particles arrive the internal diameter of the pore wall is further constricted and over time will result in the complete blockage of the pore. The mechanism is defined as Eq. (7) where $K_S$ is the fouling coefficient for the Standard blocking model.

$$\text{Standard blocking model: } J_v(t) = \frac{J_v(0)}{(1+K_S J_v(0)t)^2} \quad (7)$$

In addition to the four classic models, additional fouling models have been generated including an adsorptive fouling model that assumes particle deposition on the pore walls of the filter follows zeroth-order kinetics and is defined by Bolton et al. [9] as Eq. (8) where $K_A$ is the fouling coefficient for the Adsorption fouling model.

$$\text{Adsorptive model: } J_v(t) = J_v(0)(1-K_A J_v(0)t)^4 \quad (8)$$

For constant flow operation, the inverse of the above mentioned fouling models applies and can model the increase in pressure as a function of time by replacing $J_v(0)$ with $P_0$ as the initial pressure during constant flow mode [9].

One of the major problems with fitting a single blocking model is the assumption of a single fouling mechanism in action when in reality membrane fouling is often far more complicated and is usually better characterised using a combination of models [17,18]. The combination models enable 2 of the 5 previously discussed fouling mechanisms to act in parallel resulting in an additional ten combination fouling models to be considered. In total there were 15 different fouling models that were examined in this work and are outlined in Table 4.

To characterise the dominant fouling mechanism during constant pressure operation, a global optimisation function was implemented to find the optimum classic and combined fouling coefficients. The optimisation function minimised the summed squared error ($f(x)$) between the experimental flux decline ($J_{v,exp}$) generated at constant pressure and the predicted theoretical flux decline ($J_{v,pred}$) generated from the 15 (primary and combined) previously discussed fouling models. The optimisation function is subject to the constraint of non-negative fouling coefficients and is defined as:

$$\text{Minimise: } f(x) = \sum (J_{v,exp} - J_{v,pred})^2$$
$$\text{subject to } K_C,\ K_S,\ K_{Com},\ K_I,\ K_A \geq 0 \quad (9)$$

The dominant fouling mechanism was quantifed by the coefficient of determination ($R_{fit}^2$), calculated based on the difference between of the experimental constant pressure flux decline compared to theoretical fouling model. The coefficient of determination was defined here as:

$$R_{fit}^2 = 1 - \frac{\sum_{t=0}^{t=t}(J_{v,exp}(t)-J_{v,pred}(t))^2}{\sum_{t=0}^{t=t}(J_{v,exp}(t)-\overline{J_{v,exp}(t)})^2} \quad (10)$$

where $\overline{J_{v,exp}(t)}$ defines the mean value of the flux.

The theoretical model that best describes the observed flux decline typically defines the dominant fouling mechanism for the material. However, the fouling can often be described by multiple fouling mechanisms where the combined fouling models are typically a better fit. To demonstrate this Fig. 1 highlights an example of two experimental flux declines recorded on a depth filter for two centrates (Centrate 4 and 5) operated at constant pressure equal to 0.69 bar. The optimum theoretical flux for each experimental flux decline is shown by the solid line. Centrate 4 represented by the large pink circles was adequately described by the Cake filtration model with an $R_{fit}^2$ equal to 0.99. The primary fouling models could not accurately approximate

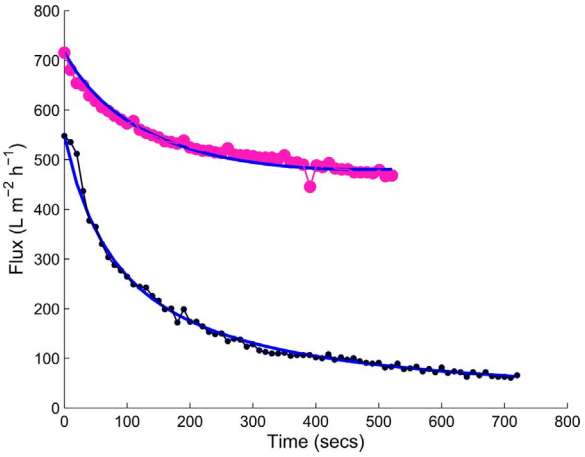


**Fig. 1.** Comparison of theoretical flux decline compared to experimental flux decline data generated from constant pressure studies using a small-scale (23 cm$^2$) depth filter. The flux decline represented by • is the experimental flux decline of Centrate 4 operated at constant pressure equal to 0.69 bar and ● represents the experimental flux decline of Centrate 5 operated at the same constant pressure. The flux represented by —— equals the optimum theoretical flux decline with the highest coefficient of determination. The best fouling model fit for Centrate 4 was the Intermediate model with $K_I$ equal to $1.942\times10^{-5}$ m$^2$ L$^{-1}$. Similar the best fouling fit model for Centrate 5 was equal to the Cake-Adsorption model with $K_C$ and $K_A$ equal to $1.085\times10^{-5}$ and $2.6\times10^{-7}$ m$^2$ L$^{-1}$. (For interpretation of the references to color in this figure, the reader is referred to the web version of this article.)

the flux decline of Centrate 5, however the combined Cake-Adsorption combined fouling model resulted in an excellent fit with $R^2_{fit}$ equal to 0.97.

## 3. Experimental materials and methods

### 3.1. Cell culture

The cell culture material utilised in these experiments was generated using Chinese Hamster Ovary (CHO) cell lines expressing a range of monoclonal antibodies (mAb) products. The cultures were produced in bench (5 L) and pilot scale (500 L) bioreactors and harvested during the decline phase of growth (days 11–14). The harvested broths had a range of cell culture properties summarised in Table 1. The cell density and cell viability were identified using an automated Trypan blue dye exclusion method (ViCell, Beckman Coulter, High Wycombe, UK).

### 3.2. Large scale centrifugation

The centrates were generated by processing the cell culture broths though a Westfalia SO1-06-107 (Odele, Germany) disk-stack centrifuge operated at 10,000 RPM and flow rates were varied between 0.3–0.9 L/min. The centrifugal operating conditions and the subsequent turbidities of the centrates are summarised in Table 2. The turbidity values recorded in this study were measured using a HACH 2100 P turbidity meter (Loveland, CO, USA).

### 3.3. Filtration

Constant pressure and constant flow filtration experiments were conducted using a 23 cm$^2$ Millistack X0HC depth filter capsule (EMD Millipore, MA, USA) with a nominal pore size ranging from 0.1 to 2 μm. The depth filter was first wetted with RO water at 200 L m$^{-2}$ h$^{-1}$ (LMH) for 20 min and subsequently aired for 10 min to remove any residual water. The centrate was well mixed using a magnetic flea and pumped through the aired filter at 100 LMH with pressure recorded for the duration of the experiment. Identical materials were used to challenge the filter in both constant pressure and constant flow approaches. During constant pressure experiments the centrate was sealed inside a feed vessel and pressurised to the set pressure using compressed air. Throughout the experiment the filtrate was collected and the volume recorded with time. A similar methodology was implemented for constant pressure operation of a 3.5 cm$^2$ Millipore SHC sterile filters (EMD Millipore, MA, USA). The pressure was set at 0.69 bar for all sterile filter experiments. A summary of the pressure set points for constant pressure operation and flowrate set point during constant flow operation are shown in Table 3.

## 4. Results and discussion

The capacity of depth filters at any scale is primarily determined by the fouling properties of the material. Understanding these characteristics faster and accurately can provide an efficient method by which to determine depth filter capacity. Capacity predictions can be performed through constant pressure operation or constant flow operation. In order to highlight the advantages of constant pressure operation compared to constant flow operation the depth filter performance was evaluated in both modes of operation using a wide range of processed materials. Processing multiple cell culture broths at a variety of centrifuge operating conditions provided a range of centrates with various fouling properties.

It is common practice in industry to quantify the capacity during constant flow operation as the total volume passed through the filter up until a given pressure drop is reached (typically 1.38 bar). This practice is however, time-consuming and material-intensive. Whilst depth filter sizing at constant pressure is not common practice, this mode of operation has the advantage of processing samples more quickly than when operating at constant flow mode. The savings of experimental process time are highlighted in Fig. 2A where the time to filter 100 mL of each centrate under both constant pressure and constant flow operation is shown. As expected all of the centrates were processed by the 23 cm$^2$ filter in approximately 26 min during constant flow operation. Constant pressure operation allows the material to be processed significantly faster, with on average an 80% reduction in processing time observed for the majority of the centrates compared to constant flow operation. Additionally, the total volume required to conduct experiments under both modes of operations is summarised in Fig. 2B and highlights an average of 70% savings of material to perform these experiments at constant pressure operation. The processing time and volume required to filter Centrate 4 with an NTU value of 560 is shown here to behave abnormally in comparison to the other five centrates. This high NTU value is atypical and resulted in rapid fouling of the filter in both modes of operation. However, filtering this turbid material under constant pressure operation mode was still faster than constant flow operation.

The significant savings in material and processing time achieved during constant pressure operation provided the impetus for developing a constant pressure operation based method to enable accurate predictions of capacity for constant flow operations. Little research has been carried out on the ability to utilise constant pressure data to enable accurate predictions of process performance of depth filters

**Table 1**
Cell culture properties of material used for constant flow and constant pressure experiments.

| Product | Material ID | Bioreactor size (L) | Cell density×10$^6$ (cells/mL) | Cell viability (%) |
|---|---|---|---|---|
| mAb-A | Centrate 1 | 500 | 25 | 68 |
| mAb-B | Centrate 2 | 5 | 20 | 75 |
| mAb-B | Centrate 3 | 5 | 20 | 75 |
| mAb-B | Centrate 4 | 5 | 20 | 75 |
| mAb-C | Centrate 5 | 500 | 24 | 90 |
| mAb-C | Centrate 6 | 500 | 24 | 90 |

**Table 2**
Centrifugal operational settings for processing of cell cultures and the resultant centrate turbidity.

| Material ID | Centrifuge flow rate (L/min) | Turbidity (NTU) |
|---|---|---|
| Centrate 1 | 0.3 | 234 |
| Centrate 2 | 0.3 | 215 |
| Centrate 3 | 0.6 | 331 |
| Centrate 4 | 0.9 | 560 |
| Centrate 5 | 0.3 | 102 |
| Centrate 6 | 0.9 | 106 |

Note: NTU-Normalised turbidity units

**Table 3**
Experimental conditions for constant flow and constant pressure studies.

| Material ID | Constant pressure operation conditions (bar) | Flowrate (LMH) |
|---|---|---|
| Centrate 1 | 0.69, 1.03, 1.38, 1.72 | 100 |
| Centrate 2 | 0.69, 1.03, 1.38, 1.72 | 100 |
| Centrate 3 | 0.69, 1.03, 1.38, 1.72 | 100 |
| Centrate 4 | 0.69, 1.03, 1.38, 1.72 | 100 |
| Centrate 5 | 0.69, 1.03 | 100 |
| Centrate 6 | 0.69, 1.03, 1.38 | 100 |

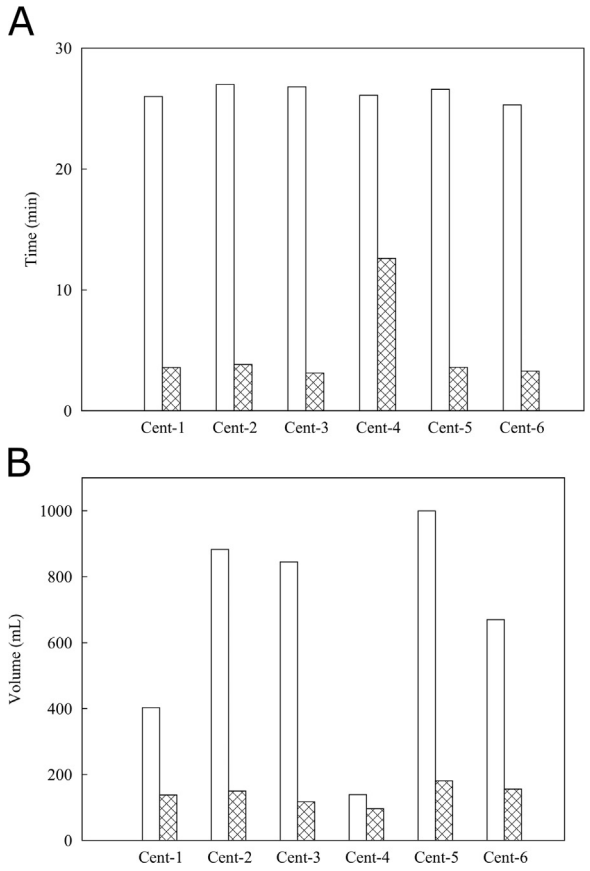


**Fig. 2.** Comparison of constant flow and constant pressure modes of operation on **(A)** experimental time to process 100 mL of material and **(B)** total process material volume requirements across multiple centrates. Centrates used by these studies were sourced from multiple cell culture broths (Table 1) and processed through a pilot scale centrifuge at a range of conditions (Table 2). Constant pressure represented as ⊠ and constant flow as □.

when operated at constant flow. The methodology reported in this paper analysed both constant pressure and constant flow depth filtration performance data. The study utilised a wide range of centrates generated from three different products and two scales as summarised

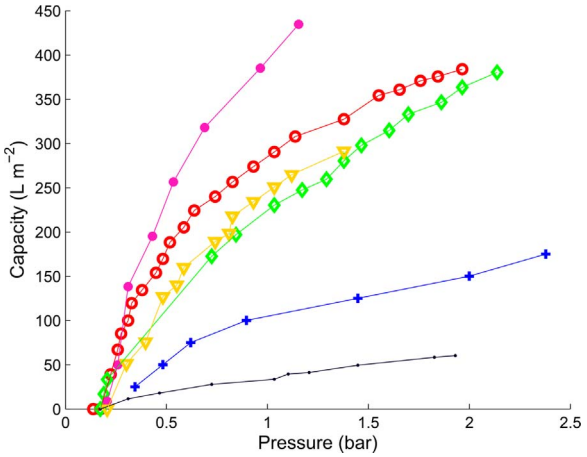


**Fig. 3.** Experimental pressure profile data generated from constant flow studies using a small-scale (23 cm$^2$) depth filter operated at 100 LMH with Centrate 1 represented as +, Centrate 2 as O, Centrate 3 as ♦, Centrate 4 as •, Centrate 5 as ● and Centrate 6 as ▼.

in Table 1. The varied range of turbidities and process characteristics of the six centrates generated a broad range of experimental capacities when operated at constant flow as shown in Fig. 3. The turbidity post centrifugation was recorded here as a quick and simple measurement to quantify centrifuge performance, similar to practices in industry [22]. It can also give a broad indication of a centrates fouling propensity during depth filtration.

As highlighted by Fig. 3, Centrate 4 with the highest turbidity (560 NTU) was shown to be the most difficult material to filter. Similarly, Centrate 5 with the lowest turbidity (102 NTU) was easily filtered and displayed a significantly higher subsequent filter capacity than the other centrates. However, Centrate 6 (106 NTU) with a similar NTU value to Centrate 5 displayed a very different level of filterability. This suggests no obvious correlation can be determined between the filterability of the centrate and its recorded turbidity. Thus the large range of observed capacities posed a real challenge in the optimum sizing of this key unit operation.

Comparable variation was observed when the six centrates were passed through the depth filter at constant pressure. The unique flux profiles for each centrate are shown in Fig. 4 highlighting the differing rates of membrane fouling specific to each material. Similar to the work carried out by Sampath et al. [18] on depth filtration of a therapeutic product expressed in a *Pichia pastoris* fermentation under constant pressure, no correlation was determined between the filterability of the centrate and the recorded turbidity. The initial flux ($J_v(0)$) of each centrate was shown to increase (Fig. 4) with pressure of operation due to the incompressible nature of the depth filter over the experimental pressure range of 0.69–1.72 bar. Similar observations were seen by Ho and Zydney [13] during microfiltration studies of bovine serum albumin solutions and by Chellam and Xu [10] during microfiltration of bacteria, colloidal silica and treated natural waters.

Characterising the fouling mechanisms observed during both modes of operation are routinely defined through the application of various mathematical fouling models as summarised in Section 2 of theoretical considerations. In this work the observed fouling during constant pressure operation of Centrates 1–6 was characterised using the classic and combined fouling models.

A global optimisation function was utilised to generate the optimum coefficients of the fouling models that minimised the error between the experimental and theoretical flux declines. The goodness of fit was quantified using the coefficient of determination ($R_{fit}^2$) and is summarised in Table 4. Of the classic models the Cake and Intermediate models were the dominant fouling mechanism found to model accurately the majority of the different flux profiles. Similarly, for the combined models, the Cake-Adsorption, Cake-Intermediate, Cake-

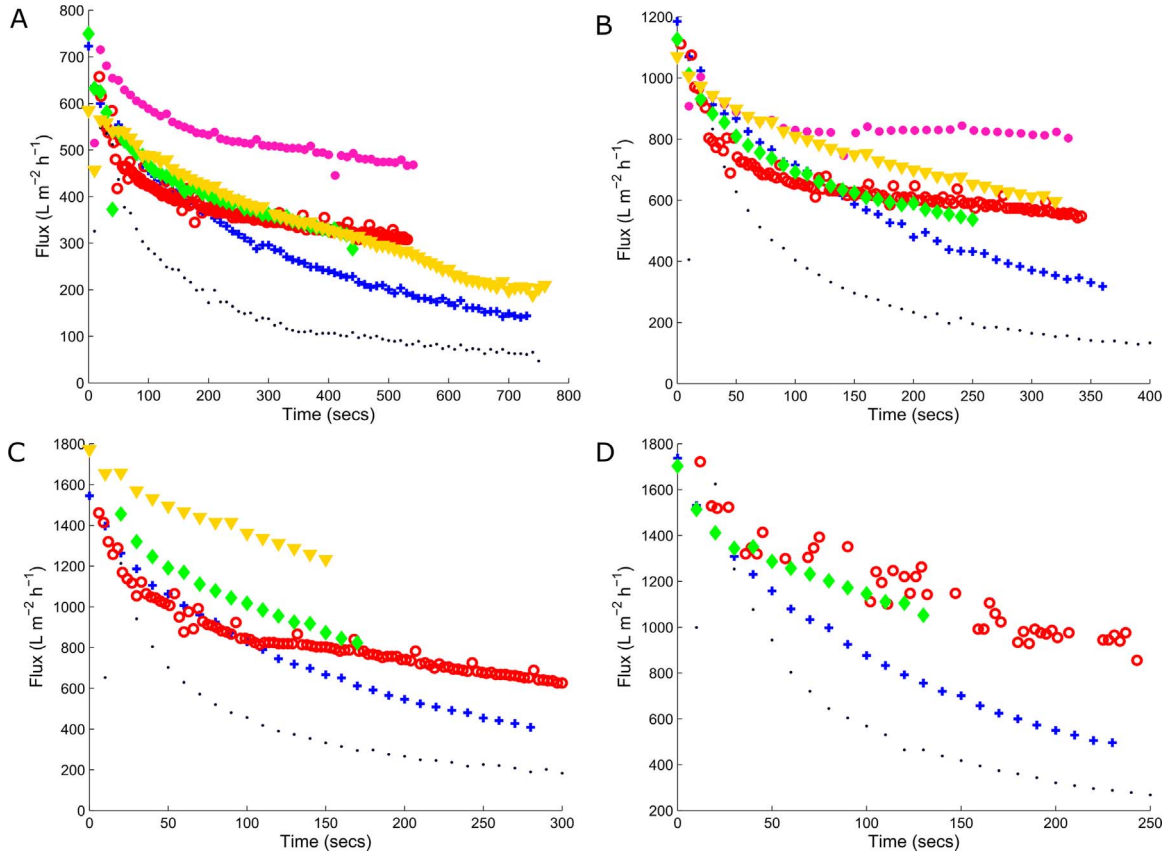


**Fig. 4.** Experimental data generated from constant pressure studies using a small-scale (23 cm$^2$) depth filter for Centrates 1–6 at pressures equal to **(A)** 0.69 bar, **(B)** 1.03 bar, **(C)** 1.38 bar and **(D)** 1.72 bar. Centrate 1 represented as blocking +, Centrate 2 as O, Centrate 3 as ♦, Centrate 4 as •, Centrate 5 as ● and Centrate 6 as ▼.

Complete and Cake-Standard were shown to model effectively the observed fouling of each centrate at the different pressures investigated. Table 4 highlights the challenge with fitting theoretical fouling models to a wide range of centrates and the inability of some of the classic models to capture the observed complex fouling mechanisms. Furthermore, some of the centrates were adequately described by two or more of the classic fouling models demonstrating the similarly between the theoretical flux declines generated by the different fouling models.

Interestingly in Table 4, the pressure was also shown to influence the blocking mechanism observed for each material. At the lower pressures where particles would be depositing onto the filter surface at a slower rate the Cake filtration model, the dominant fouling model for these materials, failed to describe adequately the fouling. This implies that in addition to the formation of the cake resistance layer there was a second type of fouling occurring. The complex fouling observed for Centrate-2 and Centrate-5 could not be described by a single fouling mechanism at the lower pressures. The Cake-Adsorption model was the only model that could adequately describe the fouling profiles observed for these centrates across all of the pressures investigated. Sampath et al. [18] reported similar findings and concluded that neither of the classic or combined fouling models could consistently fit the various flux declines for different depth filters. Although, the Cake-Adsorption model was not investigated in their work.

The optimised fouling coefficients that best described the constant pressure flux decline of Centrates 1–5 (shown in Fig. 4) were selected as the calibration dataset. The coefficients were normalised by pressure and correlated with the corresponding capacity achieved during constant flow (shown in Fig. 3) at the specific pressure investigated. For the classic models, containing a single coefficient, a simple exponential relationship generated the strongest correlation between the constant flow capacities and enabled accurate predictions. This type of relationship was selected across all of the classic models based on minimising the coefficient of determination ($R_{Cal}^2$) between the predicted and experimentally recorded capacity at constant flow for the calibration datasets (Centrates 1–5). The robustness of the correlation model was estimated by a cross validation method that estimated the performance of the model trained with one of the centrates removed from the calibration dataset and is defined in Table 5 as $R_{Cross}^2$. For the combined models, containing two coefficients, a quadratic linear regression model that considered the interaction between the two terms was assumed and a stepwise regression approach implementing both forward addition and backward elimination was used to generate the final model. The selection criteria for the finalised combined model was the same as for the classic models. A summary of the finalised correlation models of both the classic and combined models outlining their structure and prediction accuracy are shown in Table 5.

Table 5 suggests that of the classic models the correlation generated from the Cake model fouling coefficients enabled the best prediction of the constant flow capacity. However, the correlation generated from the Cake-Adsorption combined model gave a better prediction of the capacity at constant flow. This fouling mechanism suggests the dominant mechanism involves an initial deposition of the foulant onto the filter with a gradual build-up of a cake layer increasing the resistance to flow. Table 5 demonstrates that in addition to the Cake-Adsorption model, some of the other models were comparable in terms of their respective fits and power of prediction. The exponential relationship generated by the Cake model is defined in Eq. (11) where $CF_{cap,\,i}$ is the predicted filter capacity at pressure $i$ when operated at constant flow. $K_{C,\,i}$ is the Cake filtration coefficient calculated from the flux decline data when operated at constant pressure. $a$ and $b$ are calculated model coefficients.

$$CF_{cap,i} = ae^{bK_{C,i}} \tag{11}$$

**Table 4**
Summary of the classic and combined fouling model fits for Centrates 1–6 (Table 2) at the range of pressures tested (Table 3).

| CP Pressure (bar) | Intermediate | Cake | Standard | Complete | Adsorption | Cake-Adsorption | Cake-Intermediate | Complete-Standard | Intermediate-Standard | Intermediate-Adsorption | Complete-Adsorption | Cake-Complete | Intermediate-Complete | Cake-Standard | Standard-Adsorption |
|---|---|---|---|---|---|---|---|---|---|---|---|---|---|---|---|
| **Centrate 1** | | | | | | | | | | | | | | | |
| 0.69 | 0.98 | 0.96 | 0.95 | 0.87 | 0.79 | 0.96 | 0.99 | 0.95 | 0.98 | 0.98 | 0.87 | 0.99 | 0.98 | 0.99 | 0.95 |
| 1.03 | 0.99 | 0.97 | 0.98 | 0.94 | 0.90 | 0.97 | 0.99 | 0.98 | 0.99 | 0.99 | 0.64 | 1.00 | 0.99 | 0.99 | 0.98 |
| 1.38 | 1.00 | 0.97 | 0.99 | 0.95 | 0.91 | 0.97 | 1.00 | 0.99 | 1.00 | 1.00 | 0.94 | 1.00 | 1.00 | 1.00 | 0.99 |
| 1.72 | 1.00 | 0.97 | 0.99 | 0.96 | 0.92 | 0.96 | 1.00 | 0.99 | 1.00 | 1.00 | 0.96 | 1.00 | 1.00 | 1.00 | 0.99 |
| Mean | 0.99 | 0.96 | 0.98 | 0.93 | 0.88 | 0.96 | 0.99 | 0.98 | 0.99 | 0.99 | 0.85 | 1.00 | 0.99 | 0.99 | 0.98 |
| **Centrate 2** | | | | | | | | | | | | | | | |
| 0.69 | 0.05 | 0.50 | 0.00 | 0.00 | 0.00 | 0.89 | 0.50 | 0.00 | 0.02 | 0.05 | 0.00 | 0.50 | 0.05 | 0.50 | 0.00 |
| 1.03 | 0.05 | 0.48 | 0.00 | 0.00 | 0.00 | 0.92 | 0.48 | 0.00 | 0.05 | 0.05 | 0.00 | 0.48 | 0.05 | 0.48 | 0.00 |
| 1.38 | 0.69 | 0.87 | 0.54 | 0.35 | 0.23 | 0.90 | 0.87 | 0.54 | 0.69 | 0.00 | 0.35 | 0.87 | 0.69 | 0.87 | 0.54 |
| 1.72 | 0.82 | 0.86 | 0.78 | 0.73 | 0.70 | 0.87 | 0.86 | 0.78 | 0.81 | 0.82 | 0.00 | 0.86 | 0.82 | 0.86 | 0.78 |
| Mean | 0.40 | 0.68 | 0.33 | 0.27 | 0.23 | 0.90 | 0.68 | 0.33 | 0.39 | 0.23 | 0.09 | 0.68 | 0.40 | 0.68 | 0.33 |
| **Centrate 3** | | | | | | | | | | | | | | | |
| 0.69 | 0.59 | 0.78 | 0.44 | 0.23 | 0.11 | 0.77 | 0.78 | 0.44 | 0.58 | 0.59 | 0.22 | 0.78 | 0.59 | 0.78 | 0.44 |
| 1.03 | 0.89 | 0.97 | 0.83 | 0.73 | 0.67 | 0.99 | 0.97 | 0.83 | 0.89 | 0.89 | 0.73 | 0.97 | 0.89 | 0.97 | 0.83 |
| 1.38 | 0.96 | 0.99 | 0.94 | 0.91 | 0.89 | 0.99 | 0.99 | 0.94 | 0.96 | 0.96 | 0.91 | 0.99 | 0.96 | 0.99 | 0.94 |
| 1.72 | 0.86 | 0.92 | 0.81 | 0.76 | 0.74 | 0.97 | 0.92 | 0.81 | 0.86 | 0.86 | 0.70 | 0.92 | 0.86 | 0.92 | 0.81 |
| Mean | 0.83 | 0.91 | 0.75 | 0.66 | 0.60 | 0.93 | 0.91 | 0.75 | 0.82 | 0.83 | 0.64 | 0.91 | 0.82 | 0.91 | 0.75 |
| **Centrate 4** | | | | | | | | | | | | | | | |
| 0.69 | 0.99 | 0.92 | 0.97 | 0.86 | 0.76 | 0.92 | 0.99 | 0.97 | 0.99 | 0.99 | 0.85 | 0.99 | 0.99 | 0.99 | 0.97 |
| 1.03 | 1.00 | 0.96 | 0.98 | 0.90 | 0.82 | 0.96 | 1.00 | 0.98 | 1.00 | 1.00 | 0.90 | 1.00 | 1.00 | 1.00 | 0.98 |
| 1.38 | 0.99 | 0.97 | 0.95 | 0.82 | 0.70 | 0.97 | 1.00 | 0.95 | 0.99 | 0.99 | 0.81 | 1.00 | 0.99 | 1.00 | 0.95 |
| 1.72 | 1.00 | 0.97 | 0.96 | 0.85 | 0.75 | 0.97 | 1.00 | 0.96 | 1.00 | 1.00 | 0.00 | 1.00 | 1.00 | 1.00 | 0.96 |
| Mean | 0.99 | 0.96 | 0.96 | 0.86 | 0.76 | 0.96 | 1.00 | 0.96 | 0.99 | 0.99 | 0.64 | 1.00 | 0.99 | 1.00 | 0.96 |
| **Centrate 5** | | | | | | | | | | | | | | | |
| 0.69 | 0.60 | 0.74 | 0.50 | 0.40 | 0.34 | 0.97 | 0.74 | 0.50 | 0.59 | 0.60 | 0.40 | 0.74 | 0.59 | 0.74 | 0.50 |
| 1.03 | 0.00 | 0.00 | 0.00 | 0.00 | 0.00 | 0.70 | 0.00 | 0.00 | 0.00 | 0.00 | 0.00 | 0.00 | 0.00 | 0.00 | 0.00 |
| Mean | 0.30 | 0.37 | 0.25 | 0.20 | 0.17 | 0.83 | 0.37 | 0.25 | 0.30 | 0.30 | 0.20 | 0.37 | 0.30 | 0.37 | 0.25 |
| **Centrate 6** | | | | | | | | | | | | | | | |
| 0.69 | 0.98 | 0.93 | 0.99 | 0.99 | 0.98 | 0.93 | 0.99 | 0.99 | 0.99 | 0.99 | 0.99 | 0.99 | 0.99 | 0.99 | 0.99 |
| 1.03 | 0.95 | 0.99 | 0.93 | 0.88 | 0.86 | 0.99 | 0.99 | 0.93 | 0.95 | 0.95 | 0.86 | 0.99 | 0.95 | 0.99 | 0.93 |
| 1.38 | 0.96 | 0.98 | 0.95 | 0.93 | 0.92 | 0.98 | 0.98 | 0.95 | 0.96 | 0.96 | 0.93 | 0.98 | 0.96 | 0.98 | 0.95 |
| Mean | 0.96 | 0.97 | 0.95 | 0.93 | 0.92 | 0.97 | 0.98 | 0.95 | 0.97 | 0.97 | 0.92 | 0.99 | 0.97 | 0.99 | 0.95 |
| Overall mean | 0.75 | 0.81 | 0.70 | 0.64 | 0.59 | 0.93 | 0.82 | 0.70 | 0.75 | 0.72 | 0.45 | 0.82 | 0.75 | 0.82 | 0.70 |

Note: The fit is quantifed by the coefficient of determination ($R_{fit}^2$), calculated based on the difference between of the experimental constant pressure flux decline compared to theoretical fouling model. CP Pressure stands for pressure set in constant pressure mode

Whereas the Cake-Adsorption model and is defined as Eq. (12) where $K_{C,i}$ and $K_{A,i}$ are the cake and adsorptive model coefficients calculated from flux decline data when operated at constant pressure. $\alpha_0$, $\alpha_1$, $\alpha_2$ and $\alpha_3$ are the calculated model coefficients.

$$CF_{cap,i} = \alpha_0 + \alpha_1 K_{C,i} + \alpha_2 K_{A,i} + \alpha_3 K_{C,i}^{\ 2} \quad (12)$$

All of the models were found to be robust through cross validation analysis of the five centrates resulting in a high cross validation ($R_{Cross}^2$) value as summarised in Table 5. To verify further the accuracy of both models in this work, the constant flow capacity data of Centrate-6 (not included in the model calibration dataset) was implemented as an external validation dataset. The predictions were made using the calculated fouling coefficients of each model that best fitted the pressure flux profile of the Centrate-6 at 0.69, 1.03 and 1.38 bar during constant pressure operation shown in Fig. 4A–C. The generated fouling coefficients were then inserted into Eqs. (11) and (12) to predict the capacity at each pressure analysed. Fig. 5 shows the

**Table 5**
Correlation model structure and $R^2$ values for both classic and combined models.

| Fouling model | Correlation model structure | $R_{Cal}^2$ | $R_{Cross}^2$ |
|---|---|---|---|
| Intermediate | $ae^{bK_I}$ | 0.81 | 0.78 |
| Cake | $ae^{bK_C}$ | 0.83 | 0.82 |
| Standard | $ae^{bK_S}$ | 0.78 | 0.74 |
| Complete | $ae^{bK_{Com}}$ | 0.74 | 0.69 |
| Adsorption | $ae^{bK_A}$ | 0.59 | 0.59 |
| Cake-Adsorption | $\alpha_O+\alpha_1K_C+\alpha_2K_A+\alpha_3K_C^2$ | 0.86 | 0.89 |
| Cake- Intermediate | $\alpha_0+\alpha_1K_C+\alpha_2K_I+\alpha_3K_I^2$ | 0.76 | 0.79 |
| Comp-Standard | $\alpha_0+\alpha_1K_S+\alpha_2\ K_S^2$ | 0.74 | 0.72 |
| Intermediate- Standard | $\alpha_0+\alpha_1K_I+\alpha_2K_S+\alpha_2\ K_I^2$ | 0.77 | 0.76 |
| Intermediate- Adsorption | $\alpha_0+\alpha_1K_I+\alpha_2K_A+\alpha_3K_I^2+\alpha_4K_A^2$ | 0.78 | 0.75 |
| Complete-Adsorption | $\alpha_0+\alpha_1K_{Com}+\alpha_2K_A$ | 0.41 | 0.43 |
| Cake-Complete | $\alpha_0+\alpha_1K_C+\alpha_2K_{Com}+\alpha_3K_C^2$ | 0.81 | 0.81 |
| Intermediate-Complete | $\alpha_0+\alpha_1K_I+K_{Com}+\alpha_2K_I^2$ | 0.77 | 0.76 |
| Cake-Standard | $\alpha_0+\alpha_1K_C+\alpha_2K_S+\alpha_3K_C^2$ | 0.78 | 0.80 |
| Standard-Adsorption | $\alpha_0+\alpha_1K_I+\alpha_2K_I^2$ | 0.74 | 0.72 |

Note: $R_{Cal}^2$ was the coefficient of determination between the predicted and experimentally recorded capacity of the calibration dataset (Centrates 1–5). $R_{Cross}^2$ was taken as the cross validation coefficient of determination of the calibration dataset. In the correlation model structure, $K_I$, $K_C$, $K_S$, $K_{Com}$ and $K_A$ represent the model coefficients of the Intermediate, Cake, Standard, Complete and Adsorption models respectively and $a$ and $b$ are the model coefficients related to the exponential function. In the combined models, $\alpha_O$ is the intercept term and $\alpha_{1,2,3,4}$ represent the parameter coefficients of the model.

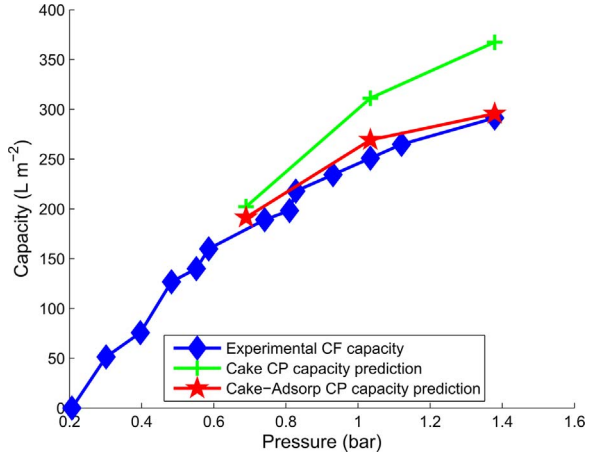


**Fig. 5.** Capacity predictions of the Cake and Cake-Adsorption fouling models for Centrate 6 at constant flow using constant pressure data recorded at 0.69, 1.03 and 1.38 bar. The experimental capacity for Centrate 6 generated in constant flow mode is shown for comparison and represented as ♦. The Cake model predictions are represented as + and the Cake-Adsorption model as ★. The symbols represent the experimental data points. The $a$ and $b$ coefficients in the Cake model were equal to 424 L m$^{-2}$ h and $-7.18\times10^5$ L m$^{-2}$, respectively and the Cake filtration coefficients recorded at constant pressure were $1.03\times10^{-6}$ ,$4.32\times10^{-7}$ and $2.01\times10^{-7}$ for each pressure investigated. For the Cake-Adsorption model, $a_O$, $a_1$, $a_2$, $a_3$ were equal to 296 L m$^{-2}$ h$^{-1}$, $-1.12\times10^8$ L$^2$ m$^{-4}$ h$^{-1}$, $6.12\times10^9$ L$^2$ m$^{-4}$ h$^{-1}$ and $9.91\times10^{12}$ L$^4$ m$^{-6}$ h, respectively. The fouling Cake-Adsorption coefficients for each pressure were equal to $1.03\times10^{-6}$,0; $5.32\times10^{-7}$, $4.86\times10^{-9}$; $2.73\times10^{-7}$, $4.80\times10^{-9}$. All fouling coefficient units are equal to m$^2$ L$^{-1}$.

predicted capacities at constant flow operation obtained from both of the correlation models. Although the Cake model is shown to predict adequately the capacity at constant flow for this centrate, the Cake-Adsorption model generates a more accurate prediction. The constant pressure flux profile generated at 1.38 bar for Centrate-6 was generated in 2.5 min and required a total of 140 mL of centrate. Filtering Centrate-6 through constant flow operation took a total of 173 min and required 670 mL to generate a capacity prediction up to 1.38 bar. Therefore, for this particular centrate the constant pressure methodology was almost 70 times quicker and required only a fraction (1/5) of the material needs of the constant flow approach.

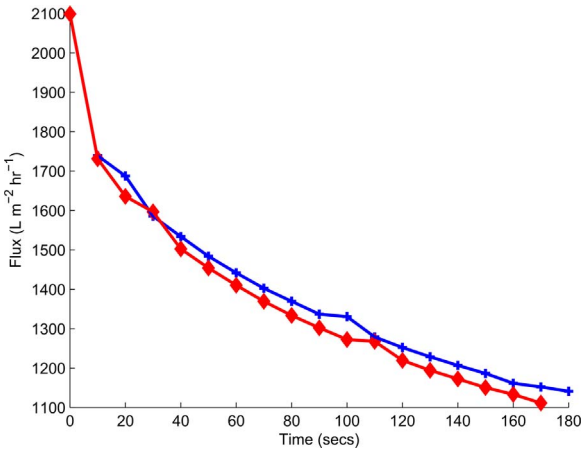


**Fig. 6.** Comparison of flux declines generated from a sterile filter when processing Centrate 6 filtrate post depth filter generated at constant pressure operation ♦ and at constant flow operation +.

It is important when creating an alternative method for filter rating that the properties of the filtrates produced by either method of operation (constant flow or constant pressure) be comparable in terms of subsequent processing. To test the ability of each method to create essentially identical filtrates, the filtrate of Centrate 6 operated at constant flow and constant pressure modes of operation were taken forward for sterile filtration. The recorded turbidites post depth filter operated at constant flow resulted in a filtrate with a turbidity equal to 23.4 NTU and at constant pressure equal to 22.8 NTU. Furthermore, Fig. 6 shows that identical flux decline profiles were generated when operating the sterile filter using material from the depth filtration step operated at both conditions. The external validation of this methodology data was carried out using Centrate 6 and validated the correlation developed. It also suggests that the developed methodology based on constant pressure operation can be utilised to characterise subsequent sterile filtration operations.

A summary outlining the new methodology is shown in Fig. 7. Firstly, the fouling coefficients for the different centrates at various constant pressures are calculated. The dominant fouling mechanism is then calculated by analysing the optimum fit of each of the classic and combined fouling models. Subsequently the capacity using the same centrates are calculated for constant flow operation up to a predefined pressure (typically 1.38 bar). A correlation is developed between the fouling coefficient of the dominant fouling mechanism and the subsequent capacity at each pressure investigated. Correlations involving the classic models can be generated using an exponential function and a linear regression model can be used for the combined model coefficients. The generated correlations can be used to predict the capacity at constant flow operation by calculating the fouling coefficient during constant pressure operation. The reduction of experimental runs and the minimisation of material requirements are the key aspect of the methodology described in Fig. 7. This study used 5 distinct feed stocks at a range of pressures to develop the correlation to successfully predict the capacity of the X0HC filter at constant flow. A possible limitation of the study is the application of a brute force modelling approach to characterise the dominant fouling mechanism based on the available classical and combined fouling models. However, this methodology was found to be valid for the filtration of multiple highly varied centrate materials and across multiple operating conditions. Although, previous reports have demonstrated significant deviations in the fouling observed between constant pressure and constant flux operation for high initial pressure fluxes [7]. The methodology reported here was found to be very robust and was verified for constant flux operation at 100 LMH. Therefore, the proposed methodology is highly

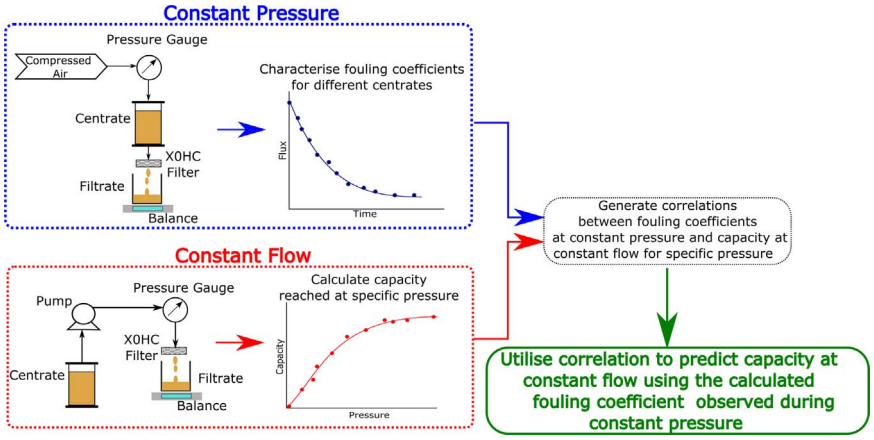


**Fig. 7.** Flow diagram summarising the development of the correlation model to predict constant flow capacity from constant pressure flux decline data.

suited to predict constant flux capacity for industrial depth-filtration operations that are typically operated at 100 LMH up to a maximum pressure differential pressure equal to 1.38 bar.

To further verify the method described in this publication an additional study on a D0HC depth filter (EMD Millipore, MA, USA) with a wider nominal pore size was conducted. The study utilised a wide range of cell culture material as feed-stock to challenge the depth filter. Fig. 1 Supplementary information highlights a strong correlation between the capacities reached at 0.69 bar for the D0HC depth filter when operated at constant flow and the standard fouling coefficients calculated for the constant pressure operation recorded at 0.69 bar. The developed correlation successfully predicted the D0HC capacities when processing three independent cell culture materials at constant flow as shown in Fig. 2 Supplementary information. The results from this study demonstrates the robustness and applicability of this methodology to work across a range of filter types and feed stocks. Furthermore, the accurate predictions of capacity at constant flow generated through constant pressure experimentation enables significant reductions in material and time requirements for various filtration studies.

## 5. Conclusion

This publication describes the development and testing of a methodology to utilise constant pressure fouling data to predict capacity during constant flow processes of depth filters using mammalian cell culture material with a range of fouling propensities. The Cake-Adsorption fouling model was found to represent accurately the dominant fouling mechanism for the wide variety of centrates analysed across the multiple pressures. The calculated coefficients of this model were highly correlated ($R_{Cal}^2$=0.86) with the capacity at constant flow for the equivalent pressure. The correlation model can be implemented to provide an accurate prediction of the capacity during constant flow operation at a specific pressure utilising the fouling coefficient calculated for the constant pressure flux profile at the specific pressure investigated. The correlation was found to be robust through cross-validation and was externally validated resulting in accurate capacity predictions of constant flow operation. The method described in this publication was also utilised to successfully predict the capacity of an alternate depth filter with a wider nominal pore size when operated at constant flow, further verifying the utility of the methodology developed. Additionally, it was also found that the filtrate generated from both modes of operation had similar qualities in terms of turbidity and subsequent sterile filter fouling propensities. The use of constant pressure over constant flow operation enabled significant savings in time and material requirements allowing for faster process development times in industry for depth filtration characterisation.

## Acknowledgement

Financial support from the UK Engineering and Physical Sciences Research Council (EPSRC) and MedImmune for the Engineering Doctorate studentship for A. Joseph is gratefully acknowledged. This research is associated with the joint UCL-MedImmune Centre of Excellence for predictive multivariate decision-support tools in the bioprocessing sector and financial support from MedImmune and UCL for S. Goldrick is gratefully acknowledged. Grant code for this work is: EP/G034656/1.

## Appendix A. Supporting information

Supplementary data associated with this article can be found in the online version at doi:10.1016/j.memsci.2017.03.002.

## References

[1] A.D. Bandaranayake, S.C. Almo, Recent advances in mammalian protein production, FEBS Lett. 588 (2014) 253–260.
[2] D.J. Roush, Y. Lu, Advances in primary recovery: centrifugation and membrane technology, Biotechnol. Prog. 24 (2008) 488–495.
[3] Y. Yigzaw, R. Piper, M. Tran, A.A. Shukla, Exploitation of the adsorptive properties of depth filters for host cell protein removal during monoclonal antibody purification, Biotechnol. Prog. 22 (2006) 288–296.
[4] R. Kempken, A. Preissmann, W. Berthold, Assessment of a disc stack centrifuge for use in mammalian cell separation, Biotechnol. Bioeng. 46 (1995) 132–138.
[5] D. Yavorsky, R. Blanck, C. Lambalot, R. Brunkow, The clarification of bioreactor cell cultures for biopharmaceuticals, Pharm. Biotechnol. 27 (2003) 62–67.
[6] F. Badmington, R. Wilkins, M. Payne, E.S. Honig, Vmax testing for practical microfiltration train scale-up in biopharmaceutical processing, Pharm. Biotechnol. 19 (1995) 64–76.
[7] D.J. Miller, S. Kasemset, D.R. Paul, B.D. Freeman, Comparison of membrane fouling at constant flux and constant transmembrane pressure conditions, J. Membr. Sci. 454 (2014) 505–515.
[8] D.M. Kanani, R. Ghosh, A constant flux based mathematical model for predicting permeate flux decline in constant pressure protein ultrafiltration, J. Membr. Sci. 290 (2007) 207–215.
[9] G.R. Bolton, A.W. Boesch, M.J. Lazzara, The effects of flow rate on membrane capacity: development and application of adsorptive membrane fouling models, J. Membr. Sci. 279 (2006) 625–634.
[10] S. Chellam, W. Xu, Blocking laws analysis of dead-end constant flux microfiltration of compressible cakes, J. Colloid Interface Sci. 301 (2006) 248–257.
[11] A. Joseph, B. Kenty, M. Mollet, K. Hwang, S. Rose, S. Goldrick, J. Bender, S.S. Farid, N. Titchener-Hooker, A scale-down mimic for mapping the process performance of centrifugation, depth and sterile filtration, Biotechnol. Bioeng. 113 (2016) 1934–1941.
[12] C. Tien, B.V. Ramarao, Revisiting the laws of filtration: an assessment of their use in identifying particle retention mechanisms in filtration, J. Membr. Sci. 383 (2011) 17–25.
[13] C.-C. Ho, A.L. Zydney, A combined pore blockage and cake filtration model for protein fouling during microfiltration, J. Colloid Interface Sci. 232 (2000) 389–399.
[14] M. Hlavacek, F. Bouchet, Constant flowrate blocking laws and an example of their application to dead-end microfiltration of protein solutions, J. Colloid Interface Sci. 82 (1993) 285–295.
[15] W. Bowen, J. Calvo, A. Hernández, Steps of membrane blocking in flux decline during protein microfiltration, J. Colloid Interface Sci. 101 (1995) 153–165.

[16] M. Said, A. Ahmad, A.W. Mohammad, M.T. Nor, S.R. Abdullah, Blocking mechanism of PES membrane during ultrafiltration of POME, J. Ind. Eng. Chem. 21 (2015) 182–188.
[17] G. Bolton, D. LaCasse, R. Kuriyel, Combined models of membrane fouling: development and application to microfiltration and ultrafiltration of biological fluids, J. Membr. Sci. 277 (2006) 75–84.
[18] M. Sampath, A. Shukla, A.S. Rathore, Modelling of filtration processes—microfiltration and depth filtration for harvest of a therapeutic protein expressed in pichia pastoris at constant pressure, Bioengineering 1 (2014) 260–277.
[19] M.E. Laska, R.P. Brooks, M. Gayton, N.,S. Pujar, Robust scale-up of dead end filtration: impact of filter fouling mechanisms and flow distribution, Biotechnol. Bioeng. 92 (2005) 308–320.
[20] C. Tien, B.V. Ramarao, Revisiting the laws of filtration: an assessment of their use in identifying particle retention mechanisms in filtration, J. Membr. Sci. 383 (2011) 17–25.
[21] P.H. Hermans, H.L. Bredee, Zur kenntnis der filtrationsgesetze, Recl. Trav. Chim. Pays-Bas. 54 (1935) 680–700.
[22] M. Westoby, J.K. Rogers, R. Haverstock, J. Romero, J. Pieracci, Modelling industrial centrifugation of mammalian cell culture using a capillary based scale-down system, Biotechnol. Bioeng. 108 (2011) 989–998.